Three-dimensional line-field Fourier domain optical coherence tomography for *in vivo* dermatological investigation

Yoshiaki Yasuno
Takashi Endo
Shuichi Makita
Gouki Aoki
Masahide Itoh
Toyohiko Yatagai
University of Tsukuba
Institute of Applied Physics
Tennodai 1-1-1, Tsukuba
Ibaraki 305-8573, Japan
E-mail: yasuno@optlab2.bk.tsukuba.ac.jp

Abstract. We demonstrate 3-D optical coherence tomography using only 1-D mechanical scanning. This system uses the principle of Fourier domain optical coherence tomography for depth resolution, 1-D imaging for lateral vertical resolution, and mechanical scanning by a galvanometer for lateral horizontal resolution. An *in vivo* human fingerpad is investigated in three dimensions with an image size of 480 points (vertical) × 300 points (horizontal) × 1024 points (depth), which corresponds to 2.1×1.4×1.3 mm. The acquisition time for a single cross section is 1 ms and that for a single volume is 10 s. The system sensitivity is 75.6 dB at a probe beam power of 1.1 mW.
 [DOI: 10.1117/1.2166628]

Keywords: optical coherence tomography; Fourier domain optical coherence tomography; interferometry.

Paper 05098R received Apr. 19, 2005; revised manuscript received Aug. 21, 2005; accepted for publication Sep. 6, 2005; published online Jan. 25, 2006.

1 Introduction

Optical coherence tomography (OCT) is one of the well-developed biomedical imaging modalities for visualizing *in vivo* tissues with a depth resolution of a few micrometers.[1] In OCT, the bandwidth of the probe-beam dominates its depth resolution, which is inversely proportional to the bandwidth. Light sources with bandwidths wider than 100 nm are commercially available, and those with much wider bandwidths are available in laboratories. OCT systems with resolutions of few micrometers or submicrometers have been demonstrated[2,3] by taking advantage of the wide bandwidth.

Despite its excellent resolution, the long measurement time of OCT is its disadvantage. Since OCT is a point-detection system, 2-D mechanical scanning is required to obtain a 2-D tomogram, and this high-order mechanical scanning results in a relatively long measurement time. Although rapid scanning optical delay lines (RSODs) have dramatically reduced the measurement time,[4–6] the A-scan rate is still around few kilohertz.[7] Even if faster delay lines were devised, ensuing high-speed detection could reduce the system sensitivity, which is proportional to the light exposure time.[8,9] This trade-off between the measurement time and the sensitivity should be overcome by new modalities in order to build a high-speed and highly sensitive OCT.

Fourier domain OCT [FD-OCT or spectral domain OCT (SD-OCT)] has been studied[10,11] in recent years for this purpose. FD-OCT does not require the mechanical A-scan due to its wavelength-resolving detection system or wavelength-swept light source, and enables real-time[12] and video rate cross-sectional imaging.[13] Another advantage of FD-OCT over conventional time-domain OCT (TD-OCT) is its higher sensitivity. This has been proved both theoretically and experimentally.[8,14] These advantages of FD-OCT effectively address the mentioned trade-off. Furthermore, FD-OCT provides direct accessibility to the phase distributions of OCT images, thus enabling smart polarization sensitive FD-OCT (Refs. 15–17) and Doppler FD-OCT (Refs. 18–20). However, FD-OCT still requires a 1-D mechanical B-scan for acquiring a 2-D OCT image or a 2-D mechanical scan for acquiring a 3-D OCT volume.

Full-field OCT [FF-OCT or full-field optical coherence microscopy (FF-OCM); Ref. 21] is another innovative modality that successfully deal with the trade-off. With a single shot of an area detector, FF-OCT visualizes an *en face* image of a sample in a specified depth. This parallel detection scheme enables high resolution,[22,23] high-speed measurements,[24] with high sensitivity[23] because the exposure time of each pixel of the array detector can be identical to the measurement time for a single *en face* image. Although FF-OCT has all these advantages, it does not provide high-speed cross-sectional imaging because in FF-OCT, cross-sectional imaging is always accompanied with 3-D volume measurement by mechanical depth scanning.

In this paper, the 1-D mechanical B-scan of FD-OCT is eliminated by using[25] an imaging optics as FF-OCT (Sec. 2.2). This OCT system, referred to as line-field FD-OCT (LF-FDOCT) in this paper, visualizes a cross-sectional OCT image without any mechanical scanning. A 1-D transversal mechanical scan (C-scan) is introduced into the LF-FDOCT for 3-D imaging (Sec. 2.3) and an *in vivo* human fingerpad is investigated in three dimensions (Sec. 3). Although 3-D LF-FDOCT has been demonstrated with static mechanical samples with relatively slow measurement speed,[26] and 2-D

Address all correspondence to Yoshiaki Yasuno, Institute of Applied Physics, University of Tsukuba, Tennodai 1-1-1, Tsukuba, Ibaraki 305-8573, Japan. Tel: 81 298 53 5217. Fax: 81 298 53 5205. E-mail: yasuno@optlab2.bk.tsukuba.ac.jp

1083-3668/2006/11(1)/014014/7/$22.00 © 2006 SPIE

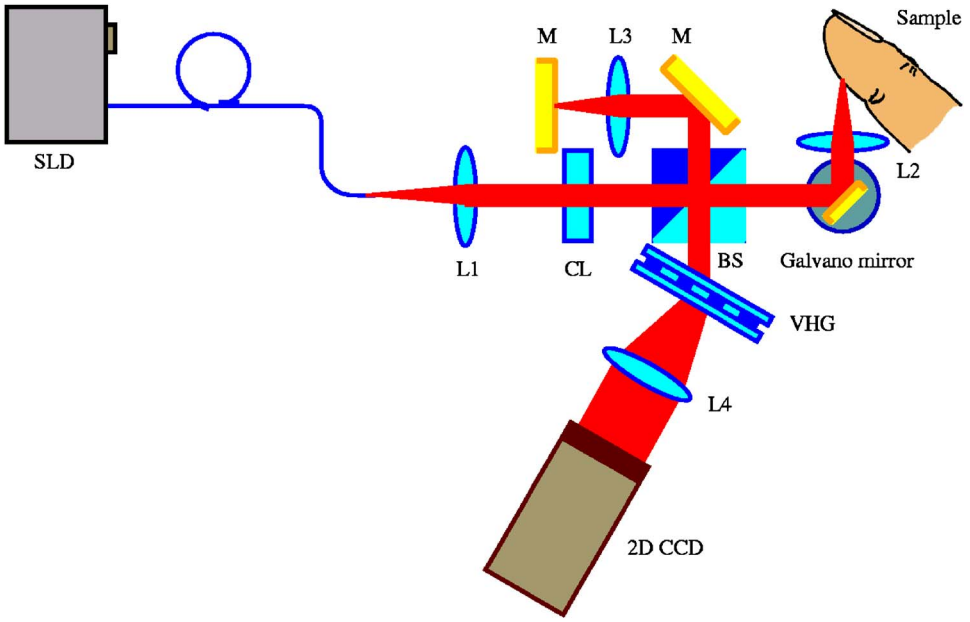

Fig. 1 Optical scheme of LF-FDOCT: Ls, lenses; CL, cylindrical lens; BS, beamsplitter: Ms; mirrors; and VHG, volume holographic grating.

LF-FDOCT has been applied to *in vivo* biological investigations,[27] to the best of our knowledge, this is the first demonstration of 3-D *in vivo* LF-FDOCT. The advantages of the LF-FDOCT in terms of its sensitivity and measurement time over conventional scanning OCT are discussed in Sec. 4.

2 Methods

2.1 *FD-OCT*

Figure 1 shows the optical scheme of LF-FDOCT consisting of a 2-D spectrometer, a free-space Michelson interferometer, and a cylindrical lens (CL). This scheme is nearly identical to that of conventional FD-OCT, with the exception of the cylindrical lens and the 2-D CCD. The light source is a superluminescent diode (SLD) with a center wavelength (λ_0) of 824 nm, a bandwidth of 19 nm, and maximum output power of 7 mW (BWC-SLD-11, B&W TEK Inc., Delaware, USA), and it provides a depth resolution of 11.4 μm with a refractive index of 1.38. The spectrometer consists of a VHG (1200 lp/mm, Wasatch Photonics, Inc.), an achromatic lens (L4) with a focal length of 150 mm and a diameter of 1 in. (Thorlabs, Inc.), and a 2-D CCD camera (TI-124B, Nikko Denki Tsushin Co., Ltd., Japan). The diffraction angle of the grating is optimized to maximize the diffraction efficiency. The CCD camera is an NTSC-standard 1/2-in. video camera that uses 640 pixels for spectral resolution and 480 pixels for lateral resolution (B-scan), the details of which are described later. The signals from the CCD camera are digitized into 10-bit numerical values by an NTSC frame grabber (PCI-1409, National Instruments) with a detection speed of 30 frames/s (fps). Each spectrum that is detected by the CCD camera and the frame grabber is rescaled into frequency space by spline or zero-filling interpolation,[13,28,29] then Hanning windowed, zero-filled from 640 pixels to 2048 pixels, and digitally inversely Fourier transformed on a computer to obtain a depth-resolved OCT image.

The relationship between the real depth and the pixel position in the image, which depends on spectrometer specifications, is examined by a plane mirror sample mounted on a micrometer. Figure 2(a) shows the 1-D OCT signals of the mirror sample with different depths, and Fig. 2(b) shows the

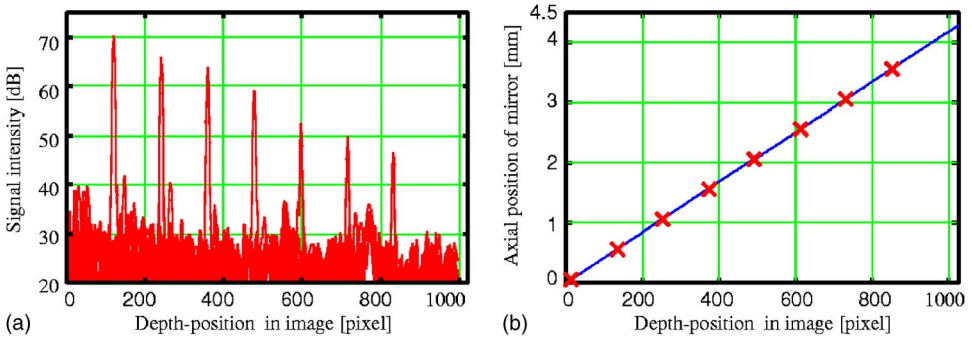

Fig. 2 (a) One-dimensional OCT signals of a mirror sample with different depths and (b) peak positions in (a) plotted against the real depth positions of the mirror sample.

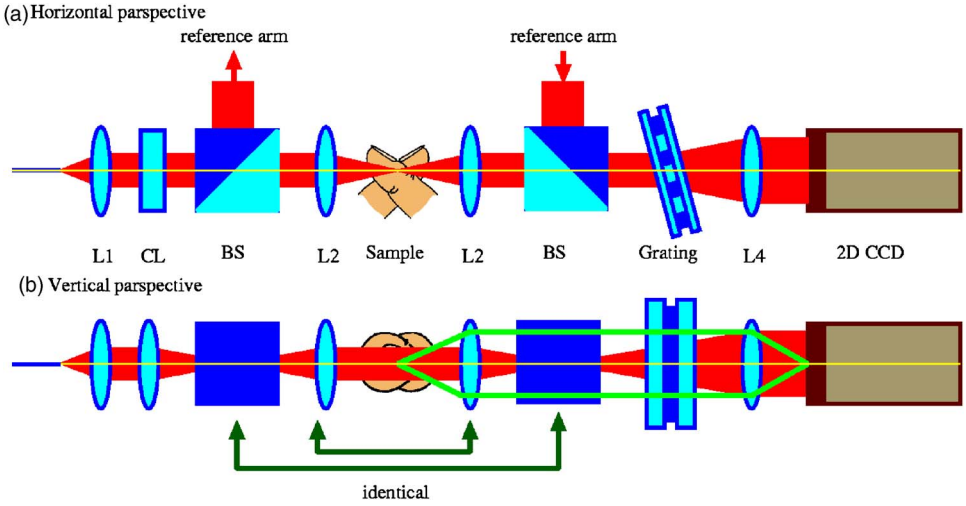

Fig. 3 (a) Horizontal and (b) vertical perspectives of optics. A reflection optics is illustrated in the form of a transmitting optics; thus, the BSs and L2s on both side of the sample are identical. Red region represents the beam shape and the green lines indicate imaging rays.

relationship between the real depth positions of the mirror sample and the peak positions of the OCT signals in terms of pixels. On the basis of the gradient of this plot, the calibration coefficient is determined to be 4.2 μm/pixel. The depth measurement range is 2048 pixels $\times$ 4.2 μm/pixel, which equals 8.6 mm. However, half of this range is occupied by mirror images,[30,31] and the effective depth-measurement range is 4.3 mm.

A theoretical effective depth-measurement range can be calculated from the parameters of the spectrometer by

$$\delta z = \frac{\lambda_0^2}{4\Delta\lambda_{\mathrm{CCD}}}, \tag{1}$$

where $\Delta\lambda_{\mathrm{CCD}}$ is the pixel spacing of the CCD in wavelength. In our LF-FDOCT, the pixel spacing of 0.04 nm/pixel yields the effective measurement range of 4.24 mm, and it agrees well with the experiment.

2.2 *Line-Field Configuration*

The LF-FDOCT does not require a mechanical A-scan due to its FD-OCT configuration. Moreover, the B-scan is not required because of line illumination and a 1-D imaging optics. As shown in Fig. 1, a CL (100-mm focal length, Sigma Koki Co., Ltd., Japan) is placed between a collimator lens [L1; a microobjective of 0.13 numerical aperture (NA), Olympus, Japan] and a beamsplitter (BS). As illustrated in Fig. 3(a), the cylindrical lens does not affect the horizontal optical perspective, and the optics is identical to that of conventional FD-OCT. On the other hand, in the vertical optical perspective, the cylindrical lens extends the illumination on the sample into a 1-D line, as shown in Fig. 3(b). The sample is then illuminated by the line focus, and the illuminated area is imaged on the CCD camera by objective L2 (an achromatic lens with a focal length of 60 mm and a diameter of 1 in., Thorlabs, Inc.) and a spectrometer-lens L4 with a transverse magnification of 2.5.

The vertical optical resolution of the LF-FDOCT system is defined by the NA of L2 by using Rayleigh's criterion:

$$\Delta y = 0.61\frac{\lambda_0}{\mathrm{NA}_{\mathrm{I2}}}, \tag{2}$$

where $\mathrm{NA}_{\mathrm{I2}}$ is the NA of L2. Based on the already mentioned parameters, the vertical optical resolution becomes $\Delta y = 2.4$ μm. Although this system has an optical resolution of 2.4 μm, the resolution is also restricted by the pixel size of the CCD camera. A single pixel of the CCD corresponds to an area with a length of 5.4 μm on the sample, hence the practical resolution is dominated by the CCD pixel size. Because of Nyquist sampling theorem, the resolution can be defined as twice the size of the CCD pixel. In our LF-FDOCT, $\Delta y = 10.8$ μm.

The vertical measurement range of the LF-FDOCT system is dominated by the magnification M and the size of the CCD, or the height of the line focus. In the proposed LF-FDOCT, the first and the second parameters dominate the measurement range of 2.6 mm, and this field is sampled by 480 pixels on the CCD.

2.3 *Configuration for 3-D Measurement*

The LF-FDOCT can measure a 2-D tomogram without mechanical scanning. To extend LF-FDOCT for 3-D measurements, we introduce a 1-D mechanical C-scan. A gold-protected mirror mounted on a 1-D galvanometer (Model 6220, Cambridge Technology) is placed at the back focal plane of L2, and it swings the probe beam horizontally. A function generator board with a 12-bit digital-to-analog resolution (DAQ-2502, ADLINK Technology, Inc.) plugged into a Windows 2000 computer generates the control signal for the galvanometer. The function generator board, and thus the galvanometer, are synchronized with the operation of the CCD camera by a trigger signal from the frame grabber. Owing to this synchronization scheme, the 3-D measurement speed of this LF-FDOCT system is limited only by the driving speed of the CCD. The B-scan rate of the 3-D acquisition is 30 B-scans/s and it is identical with that of 2-D acquisition.

The maximum horizontal measurement field—25 mm—is dominated by the maximum rotation angle of the galvanom-

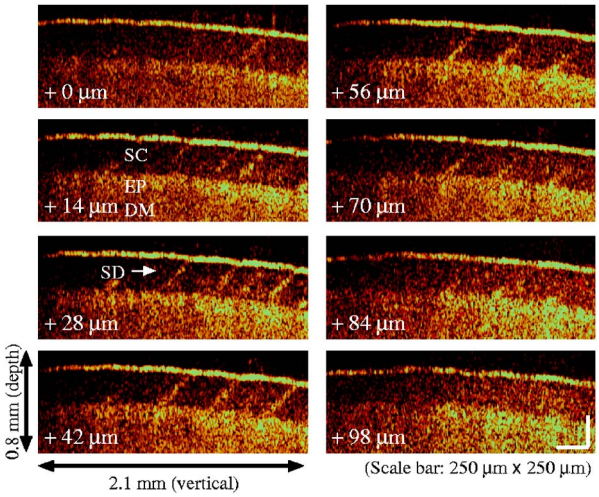

Fig. 4 Vertical cross sections of an *in vivo* human fingerpad. A single cross section is acquired from a single-shot detection: SC, stratum corneum; EP, epitherium; DM; dermis; and SD, swet a duct.

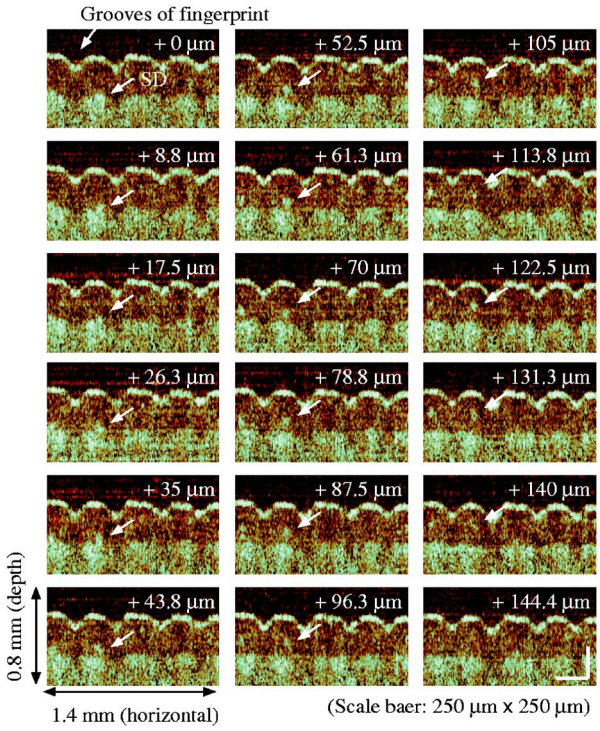

Fig. 5 Horizontal cross sections of an *in vivo* human fingerpad. The cross sections are reconstructed from the 3-D OCT volume. The white arrow points the cross section of an SD.

eter and the focal length and the diameter of L2.

The horizontal resolution is defined in the same manner as that in conventional TD-OCT and FD-OCT, i.e., it is based on probe beam diameter and the focal length of the objective. In the proposed LF-FDOCT, the horizontal resolution is 15.8 μm.

3 Results

We investigate an *in vivo* fingerpad of a healthy human volunteer (age 24, male) in three dimensions. The probe power (1.2 mW) is sufficiently weaker than the ANSI safety standard.[32] To reduce the motion artifacts, the exposure time is set to 1 ms by the electrical shutter of the CCD camera (see Sec. 4.2), and 300 B-scans are acquired in 10 s. In this investigation, the separation between adjacent B-scans is 4.8 μm and the horizontal field for the 300 B-scans is 1.44 mm. The measurement volume size is 2.1 (vertical) × 1.4 (horizontal) × 1.3 mm (depth), and the corresponding data points are 480 points (vertical) × 300 points (horizontal) × 320 points (depth).

Figure 4 shows vertical cross sections of the sample at several horizontal positions, and a single cross section is acquired from a single-shot image on the CCD. The exponential attenuation along the depth penetration is numerically compensated. The acquisition speed is 30 cross sections/s. Structures such as stratum corneum (SC), epithelium (EP), and dermis (DM) can be seen. The direction of the sectioning is parallel to the grooves of the fingerprint, thus, some sweat ducts (SDs) are aligned in a single B-scan.

Horizontal cross sections reconstructed from the 3-D volume at several vertical positions are shown in Fig. 5. In this case, the direction of the sectioning is perpendicular to the fingerprint, and the grooves of the fingerprint can be seen. A white arrow points the cross section of a sweat duct which screwing up from the dermis to the stratum corneum along a virtual horizontal scanning.

En face images reconstructed from the 3-D OCT volume are shown in Fig. 6. The ridges of the stratum corneum associated with the fingerprint are shown in the *en face* images corresponding to the depths of +0 to +160 μm. The small aligned spots in the image corresponding to the depth of +240 μm indicate SDs. The images corresponding to the

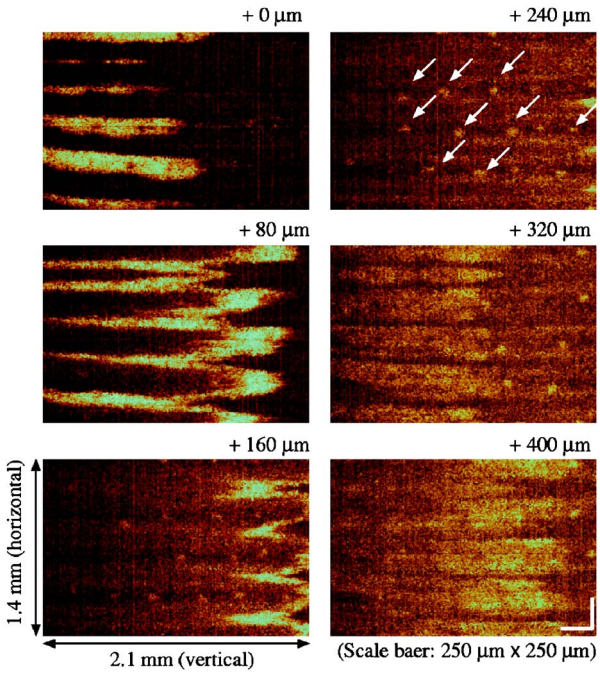

Fig. 6 Reconstructed *en face* images from the OCT volume at several depth positions.

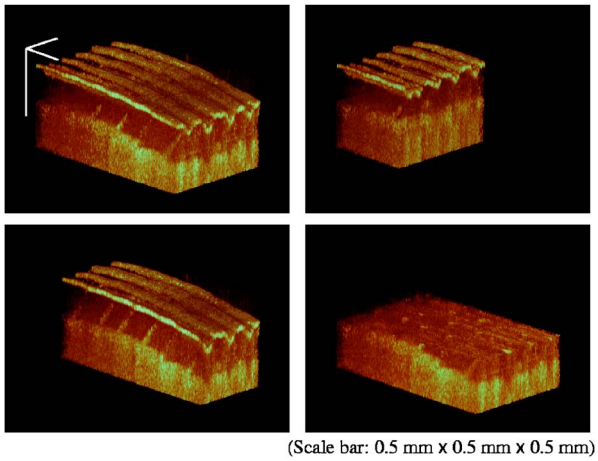

Fig. 7 Volume-rendered 3-D OCT volumes of an *in vivo* human fingerpad with several cross sections.

depths of +320 and +400 μm show the ridges between the EP and DM.

The 3-D OCT data is volume-rendered by an image processing software [etdips,[33] National Institutes of Health (NIH) Clinical Center)]. The volume-rendered results are shown in Fig. 7.

4 Discussions

4.1 *System Sensitivity*

We examine the sensitivity of the LF-FDOCT system by measuring a mirror sample with an exposure time of 1 ms, a probe power of 1.1 mW, and a probe attenuation of −36.6 dB. The dynamic range is 39 dB, therefore the system sensitivity is 75.6 dB, while the theoretical sensitivity is 83.9 dB. The degradation in the sensitivity may be due to the nonuniformity of the line illumination and vignetting of the CCD. Because an SLD is a spatially coherent light source, coherent crosstalk among the lateral points, which is not evident in the measurement of the mirror but is evident in that of biological samples, may cause additional degradation of the sensitivity. This coherent crosstalk can be suppressed by using spatially incoherent light source with a line slit, which is used to enhance the spatial coherence in one dimension, although this configuration sacrifices great portion of the optical power of the light source.

The exposure time dependency of the signal-to-noise ratio (SNR) and the sensitivity are examined, as shown in Fig. 8. Figure 8(a) reveals that the SNR is proportional to the exposure time, as theoretically predicted, and Fig. 8(b) shows the theoretical shot-noise-limited sensitivity (solid curve) and experimentally measured sensitivity (×). A formula from Ref. 9 and the following parameters are used to calculate the theoretical sensitivity; 480 pixels, 6.5% quantum efficiency of the camera, and 80% spectrometer efficiency. The fill factor of the CCD camera, which is not disclosed by its manufacturer, is assumed to be 100%. This assumption may have resulted in the disagreement between the theoretical curve and the experimental values.

As shown in Fig. 8, a longer exposure time leads to higher sensitivity, and we can use a longer exposure time in LF-FDOCT than in conventional FD-OCT. This is because in an LF-FDOCT, the exposure time can be identical to the acquisition time of a single B-scan while the maximum exposure time of a conventional FD-OCT is equal to the acquisition time of a single A-scan. Hence, in principle, the sensitivity of LF-FDOCT is greater than that of a conventional FD-OCT by a factor of $10 \log N$ dB, where N is the number of A-scans in a single B-scan. This discussion is analogous[23] to that of an FF-OCT. In our setup, the maximum gain in the sensitivity is $10 \log 480 = 26.8$ dB. However, note that the long exposure time enhances the motion artifacts and may degrade the sensitivity. The effect of the motion artifacts is discussed in the following section.

The system sensitivity also depends on the depth in the measurement field, as seen in Fig. 2(a). This figure indicates that the sensitivity at the end of the measurement range is 36 dB lower than the highest sensitivity, which is at the center of the measurement range (zero delay point). This degradation may be due to the limited resolution of the spectrometer, because the dimensions of optical elements limit the resolution so that it is slightly worse than the sufficient resolution. And the numerical error of the wavelength-frequency rescaling also may be the cause of the degradation.

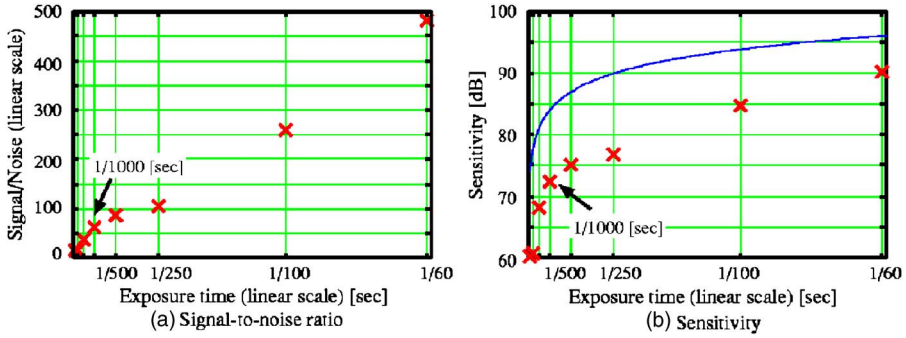

Fig. 8 (a) Experimentally measured SNR on a linear scale and (b) theoretical system sensitivity (solid curve) and experimental system sensitivity (×).

4.2 *Effect of Motion Artifacts*

Although a longer exposure time leads to the higher sensitivity, it can deteriorate the image quality because of the motion artifacts.[34]

The effect of the motion artifacts in the LF-FDOCT is identical to that in a conventional FD-OCT, however, this effect is relatively large in the former because the exposure time is longer than that in a conventional FD-OCT. On the basis of a formula derived by Yun et al.,[34] the maximum allowable velocity for the SNR decay of −10 dB along the depth is

$$\frac{0.37\lambda_0}{T} = 307\ \mu\text{m/s}, \tag{3}$$

where T is the exposure time, which is 1 ms in our case. This result suggests that the maximum displacement in the exposure time is 307 nm.

The maximum allowable lateral velocities are also calculated from the formula by Yun et al. as $\Delta y/T = 10.8$ mm/s for vertical motion and $\Delta x/T = 15.8$ mm/s for horizontal motion, where Δy and Δx are vertical and horizontal resolutions, respectively.

These estimations suggest that the LF-FDOCT is approximately 20 times more sensitive to axial sample motion than to transversal motions.

4.3 *Potential System Speed*

In the measurement described in Sec. 3, the exposure time for a single B-scan is 1 ms. Within this duration, 480 A-scans are acquired, hence, the A-scan rate of a single B-scan is 480 kHz, however, the overall A-scan rate for the 3-D measurement is 14.4 kHz because of the limited duty cyle of 3%, which is due to the fixed frame rate of the NTSC camera. However, if we use a high-speed CCD camera and a high-speed sampling device, the overall A-scan rate for 3-D measurements can be improved up to 480 kHz. This would potentially enable a 2-D OCT measurement at a rate of 1000 fps, and a 3-D OCT measurement at a rate of 3.3 volumes/s.

4.4 *Aberrations*

With the exception of the cylindrical lens, all of the lenses in the LF-FDOCT system are achromatic doublets, which are designed to correct both achromatic and monochromatic aberrations. The cylindrical lens, which is a planoconvex singlet, can cause an achromatic aberration. The spectral width at the top and bottom perimeters of the line focus can be slightly degraded by the aberration when compared to the spectral width of the light source itself. However, these perimeters are not used for the OCT measurement, therefore, the effect of the achromatic aberration is negligible.

The cylindrical lens also causes a comatic aberration. If the rays do not impinge perpendicularly on the cylindrical lens, the comatic aberration can degrade the quality of the line focus. However, the proposed LF-FDOCT is free from comatic aberration, because the rays enter the cylindrical lens perpendicularly, as shown in Fig. 3(a).

5 Conclusions

We demonstrated a new modality of 3-D OCT. This system eliminates its A-scan by using FD-OCT and avoids the mechanical B-scan by an imaging optics. The system has a depth resolution of 11.4 μm, a vertical lateral resolution of 10.8 μm, and a horizontal lateral resolution of 15.8 μm. The system sensitivity is experimentally determined to be 75.64 dB with a probe power of 1.1 mW and an exposure time of 1 ms. The A-scan rate of the system is 480 kHz for a single B-scan, while it is 14.4 kHz for a 3-D measurement.

The system visualized inner structures of an *in vivo* human fingerpad in an area of 2.1 (vertical) × 1.4 (horizontal) × 1.3 mm (depth) for 10 s. The corresponding image size is 480 points (vertical) × 300 points (horizontal) × 320 points (depth), while the maximum measurement size is 480 points (vertical) × 300 points (horizontal) × 1024 points (depth). In this measurement, the maximum allowable velocities are 307 μm/s for axial sample motion, 10.8 mm/s for vertical motion, and 15.8 mm/s for horizontal motion.

Acknowledgments

This research is partially supported by Grant-in-aid for Scientific Research No. 15760026 from the Japan Society for the Promotion of Science (JSPS), Japan Science and Technology Agency, and the Special Research Project of Nanoscience at University of Tsukuba. Shuichi Makita is supported by JSPS by a contract under the Promotion of Creative Interdisciplinary Materials Science for Novel Functions, 21st Century Center of Excellence (COE) Program. The authors wish to acknowledge Dr. Masahiro Akiba of the Yamagata Promotional Organization for Industrial Technology for helpful discussions.

References

1. D. Huang, E. A. Swanson, C. P. Lin, J. S. Schuman, W. G. Stinson, W. Chang, M. R. Hee, T. Flotte, K. Gregory, C. A. Puliafito, and J. G. Fujimoto, "Optical coherence tomography," *Science* **254**, 1178–1181 (1991).
2. W. Drexler, U. Morgner, F. X. Kartner, C. Pitris, S. A. Boppart, X. D. Li, E. P. Ippen, and J. G. Fujimoto, "*In vivo* ultrahigh-resolution optical coherence tomography," *Opt. Lett.* **24**, 1221–1223 (1999).
3. B. Povazay, K. Bizheva, A. Unterhuber, B. Hermann, H. Sattmann, A. F. Fercher, W. Drexler, A. Apolonski, W. J. Wadsworth, J. C. Knight, P. St. J. Russell, M. Vetterlein, and E. Scherzer, "Submicrometer axial resolution optical coherence tomography," *Opt. Lett.* **27**, 1800–1802 (2002).
4. G. J. Tearney, M. E. Brezinski, B. E. Bouma, S. A. Boppart, C. Pitris, J. F. Southern, and J. G. Fujimoto, "*In vivo* endoscopic optical biopsy with optical coherence tomography," *Science* **276**, 2037–2039 (1997).
5. G. J. Tearney, B. E. Bouma, and J. G. Fujimoto, "High-speed phase- and group-delay scanning with a grating-based phase control delay line," *Opt. Lett.* **22**, 1811–1813 (1997).
6. A. Rollins, J. Izatt, M. Kulkarni, S. Yazdanfar, and R. Ungarunyawee, "*In vivo* video rate optical coherence tomography," *Opt. Express* **3**, 219–229 (1998).
7. B. H. Park, M. D. Pierce, B. Cense, and J. F. de Boer, "Real-time multi-functional optical coherence tomography," *Opt. Express* **11**, 782–793 (2003).
8. R. A. Leitgeb, C. K. Hitzenberger, and A. F. Fercher, "Performance of Fourier domain vs. time domain optical coherence tomography," *Opt. Express* **11**, 889–894 (2003).
9. J. F. de Boer, B. Cense, B. H. Park, M. C. Pierce, G. J. Tearney, and B. E. Bouma, "Improved signal-to-noise ratio in spectral-domain compared with time-domain optical coherence tomography," *Opt. Lett.* **28**, 2067–2069 (2003).

10. A. F. Fercher, C. K. Hitzenbergera, G. Kampa, and S. Y. El-Zaiatb, "Measurement of intraocular distances by backscattering spectral interferometry," *Opt. Commun.* **117**, 43–48 (1995).
11. G. Häusler and M. W. Lindner, "'Coherence Radar' and 'Spectral Radar'—new tools for dermatological diagnosis," *J. Biomed. Opt.* **3**, 21–31 (1998).
12. M. Wojtkowski, T. Bajraszewski, P. Targowski, and A. Kowalczyk, "Real-time *in vivo* imaging by high-speed spectral optical coherence tomography," *Opt. Lett.* **28**, 1745–1747 (2003).
13. N. A. Nassif, B. Cense, B. H. Park, M. C. Pierce, S. H. Yun, B. E. Bouma, G. J. Tearney, T. C. Chen, and J. F. de Boer, "*In vivo* high-resolution video-rate spectral-domain optical coherence tomography of the human retina and optic nerve," *Opt. Express* **12**, 367–376 (2004).
14. N. Nassif, B. Cense, B. H. Park, S. H. Yun, T. C. Chen, B. E. Bouma, G. J. Tearney, and J. F. de Boer, "*In vivo* human retinal imaging by ultrahigh-speed spectral domain optical coherence tomography," *Opt. Lett.* **29**, 480–482 (2004).
15. Y. Yasuno, S. Makita, Y. Sutoh, M. Itoh, and T. Yatagai, "Birefringence imaging of human skin by polarization-sensitive spectral interferometric optical coherence tomography," *Opt. Lett.* **27**, 1803–1805 (2002).
16. Y. Yasuno, S. Makita, T. Endo, M. Itoh, T. Yatagai, M. Takahashi, C. Katada, and M. Mutoh, "Polarization-sensitive complex Fourier domain optical coherence tomography for Jones matrix imaging of biological samples," *Appl. Phys. Lett.* **85**, 3023–3025 (2004).
17. J. Zhang, W. Jung, J. S. Nelson, and Z. Chen, "Full range polarization-sensitive Fourier domain optical coherence tomography," *Opt. Express* **12**, 6033–6039 (2004).
18. R. A. Leitgeb, L. Schmetterer, W. Drexler, A. F. Fercher, R. J. Zawadzki, and T. Bajraszewski, "Real-time assessment of retinal blood flow with ultrafast acquisition by color Doppler Fourier domain optical coherence tomography," *Opt. Express* **11**, 3116–3121 (2003).
19. B. R. White, M. C. Pierce, N. Nassif, Barry Cense, B. H. Park, G. J. Tearney, B. E. Bouma, T. C. Chen, and J. F. de Boer, "*In vivo* dynamic human retinal blood flow imaging using ultra-high-speed spectral domain optical coherence tomography," *Opt. Express* **11**, 3490–3497 (2003).
20. R. A. Leitgeb, L. Schmetterer, C. K. Hitzenberger, A. F. Fercher, F. Berisha, M. Wojtkowski, and T. Bajraszewski, "Real-time measurement of in vitro flow by Fourier-domain color Doppler optical coherence tomography," *Opt. Lett.* **29**, 171–173 (2004).
21. E. Beaurepaire, A. C. Boccara, M. Lebec, L. Blanchot, and H. Saint-Jalmes, "Full-field optical coherence microscopy," *Opt. Lett.* **23**, 244–246 (1998).
22. L. Vabre, A. Dubois, and A. C. Boccara, "Thermal-light full-field optical coherence tomography," *Opt. Lett.* **27**, 530–532 (2002).
23. A. Dubois, K. Grieve, G. Moneron, R. Lecaque, L. Vabre, and C. Boccara, "Ultrahigh-resolution full-field optical coherence tomography," *Appl. Opt.* **43**, 2874–2883 (2004).
24. M. Akiba, K. P. Chan, and N. Tanno, "Full-field optical coherence tomography by two-dimensional heterodyne detection with a pair of CCD cameras," *Opt. Lett.* **28**, 816–818 (2003).
25. A. F. Zuluaga and R. Richards-Kortum, "Spatially resolved spectral interferometry for determination of subsurface structure," *Opt. Lett.* **24**, 519–521 (1999).
26. T. Endo, Y. Yasuno, S. Makita, M. Itoh, and T. Yatagai, "Profilometry with line-field Fourier-domain interferometry," *Opt. Express* **13**, 695–701 (2005).
27. B. Grajciar, M. Pircher, A. F. Fercher, and R. A. Leitgeb, "Parallel Fourier domain optical coherence tomography for *in vivo* measurement of the human eye," *Opt. Express* **13**, 1131–1137 (2005).
28. M. Wojtkowski, R. Leitgeb, A. Kowalczyk, T. Bajraszewski, and A. F. Fercher, "*In vivo* human retinal imaging by Fourier domain optical coherence tomography," *J. Biomed. Opt.* **7**, 457–463 (2002).
29. C. Dorrer, N. Belabas, J.-P. Likforman, and M. Joffre, "Spectral resolution and sampling issues in Fourier-transform spectral interferometry," *J. Opt. Soc. Am. B* **17**, 1795–1802 (2000).
30. M. Wojtkowski, A. Kowalczyk, R. Leitgeb, and A. F. Fercher, "Full range complex spectral optical coherence tomography technique in eye imaging," *Opt. Lett.* **27**, 1415–1417 (2002).
31. Y. Yasuno, S. Makita, T. Endo, G. Aoki, H. Sumimura, M. Itoh, and T. Yatagai, "One-shot-phase-shifting Fourier domain optical coherence tomography by reference wavefront tilting," *Opt. Express* **12**, 6184–6191 (2004).
32. American National Standards Institute, *American National Standard for the Safe Use of Lasers ANSI Z136.1-2000*, American National Standards Institute, New York (2000).
33. "etdips; a multidimensional volume visualization and analysis software," codeveloped by the National Institutes of Health (NIH) and the National University of Singapore (NUS) under CRADA (CACR-645).
34. S. H. Yun, G. J. Tearney, J. F. de Boer, and B. E. Bouma, "Motion artifacts in optical coherence tomography with frequency-domain ranging," *Opt. Express* **12**, 2977–2998 (2004).